IEEE Access
Multidisciplinary ⋮ Rapid Review ⋮ Open Access Journal

Received 14 May 2024, accepted 27 May 2024, date of publication 3 June 2024, date of current version 10 June 2024.

Digital Object Identifier 10.1109/ACCESS.2024.3408671

RESEARCH ARTICLE

Low-Loss 3D-Printed Waveguide Filters Based on Deformed Dual-Mode Cavity Resonators

MICHAL BARANOWSKI[1], (Graduate Student Member, IEEE), LUKASZ BALEWSKI[2], ADAM LAMECKI[1,2], (Senior Member, IEEE), AND MICHAL MROZOWSKI[1], (Fellow, IEEE)

[1]Department of Microwave and Antenna Engineering, Faculty of Electronics, Telecommunications and Informatics, Gdansk University of Technology, 80-233 Gdansk, Poland
[2]EM Invent Sp. z o.o., 80-172 Gdansk, Poland

Corresponding author: Michal Baranowski (michal.baranowski@pg.edu.pl)

This work was supported by the National Science Centre, Poland, under Agreement 2020/39/O/ST7/02897.

ABSTRACT This paper introduces a new type of waveguide filter with smooth profile, based on specially designed dual-mode (DM) cavity resonators. The DM cavity design is achieved by applying a shape deformation scheme. The coupling between the two orthogonal cavity modes is implemented by breaking the symmetry of the structure, thus eliminating the need for additional coupling elements. The modes operating in the cavity are carefully analyzed and a scheme for managing the spurious modes is discussed. Two filter prototypes employing the designed DM cavities are developed and described in detail. The first design is a fourth-order bandpass filter (BPF) with a 90° rotated output and a transmission zero (TZ), whereas the second design is an eighth-order filter with four TZs. Both designs are developed, taking into account the limitations of 3D printing technology to enable their single-piece fabrication without internal supports. The structures benefit from additive manufacturing (AM) by having a smooth surface profile and reduced weight, which is often highly desirable for high-power and low-loss applications. Filter prototypes were manufactured using selective laser melting (SLM) from aluminum alloy and tested to validate the designs. Measurement results are consistent with the simulation and prove the validity of the proposed solutions. Both measured BPF prototypes demonstrate low insertion loss, i.e., 0.11 dB and 0.25 dB for the fourth-order and eighth-order designs, respectively. The estimated Q-factors reach 3500 and 4500, which is a very good result for 3D-printed parts.

INDEX TERMS Additive manufacturing, design optimization, dual-mode cavity resonator, dual-mode waveguide filter, shape deformation.

I. INTRODUCTION

Additive manufacturing (AM) has become one of the key emerging technologies for efficient manufacturing of passive microwave components, such as waveguide filters, couplers and antennas [1], [2], [3], [4], [5], [6], [7], [8], [9], [10]. The use of 3D printing methods for making high-frequency electronics has grown rapidly over the last decade, due to their low cost and high flexibility in creating complex 3D models. With the advancement of professional AM processes in the industry, 3D printing can not only be used for quick prototyping, but also for professional manufacturing of high-frequency components, along with the traditional subtractive methods such as Computer Numerical Control (CNC) milling. The freedom in obtaining complex 3D structures can help overcome the limitations of the conventional manufacturing methods, thus opening the way for new solutions in microwave component design. The new microwave components developed using AM can have non-standard profiles, leading to improvements in their electromagnetic (EM) performance, such as lower loss, superior quality factor Q, wider spurious mode separation [11], [12], [13], [14], and better power handling capability and thermal stability [15]. 3D printing can also help shrink the size of systems by combining several useful functions in one component [16], [17]. However, to use AM processes

The associate editor coordinating the review of this manuscript and approving it for publication was Derek Abbott.

effectively in microwave engineering, specialized tools are required for the design, simulation, and optimization of 3D structures with complex and smooth geometries.

One way of addressing this challenge is to develop new design methods oriented toward fabrication by AM, e.g., analytic method for the synthesis of waveguide filters with a smooth profile [18]. Another possible solution focuses on adapting computer-aided design (CAD) tools, well established in microwave engineering, to provide greater freedom in 3D modeling. Enhancing conventional 3D CAD of high-frequency passive components with the shape deformation technique was presented in [19]. The geometry modification algorithm based on radial basis function (RBF) interpolation was developed and integrated with a 3D finite element method (FEM) in the EM field simulator InventSim [20], which is utilized as a main tool to optimize the presented designs. This technique makes it possible to create truly arbitrary 3D models by means of reshaping predefined basic geometries. The working principle of this method is based on manipulating a set of points defined around the object which control the deforming operation. The deformation is performed by shifting some of the control points to certain new coordinates. The original structure, treated as a 3D mesh of points, is then smoothly reshaped according to this displacement. This method was already applied to the development of several microwave filter designs and demonstrated very good results, e.g., by improving the out-of-band performance of waveguide filters [11], [19]. In this work, the shape deformation technique is applied to design smooth-profile rectangular waveguide dual-mode (DM) cavity filters suitable for direct metal additive manufacturing using the selective laser melting (SLM) process. Initially, deformation is applied to form a cavity geometry, facilitating the coupling of the two orthogonal modes together and achieving dual-mode operation in the cavities. Subsequently, this concept is further developed and employed to design a waveguide filter structure with a smooth profile, prepared for 3D printing in one piece, thereby eliminating the need for parts assembly.

Many 3D-printed filter designs implementing various cavity types have been reported in the literature, including dual- or multi-mode filter structures [15], [21], [22], [23], [24], [25], [26], [27], [28], [29], [30], [31]. Some notable examples are the designs based on spherical cavities [15], [21], ellipsoidal cavities [29], [30], or dimpled ellipsoidal cavities [31]. These designs take advantage of AM because spherical or ellipsoidal cavity shapes are often difficult to fabricate using conventional subtractive methods. However, 3-D printing of spherical cavities may result in overhangs and degraded surfaces due to the lack of internal supports, which was discussed and demonstrated in [6]. Additionally, in all the referenced DM filter designs, a coupling mechanism is needed to excite the two orthogonal cavity modes and allow for energy transfer between them. In [15], [26] and [31], internal coupling between the two modes operating in the cavity is implemented by inserting coupling elements, corner cuts or 'dimples', thereby breaking the symmetry of the cavity. In [29] and [30], however, the two modes are not coupled together, but rather excited separately by rotating the input and output ports (i.e., direct coupling from the source or load to both cavity modes). This paper addresses these issues while maintaining complex cavity geometry that can only be made by 3D printing. In the proposed method, the second cavity mode is excited by perturbing the cavity shape to get a non-symmetric cross-section, similarly to what was done in [32].

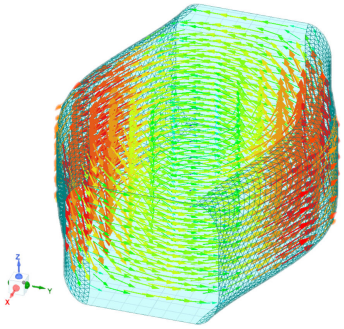

FIGURE 1. Operating fundamental TE110 mode (H field) in the basic smooth-profile rectangular waveguide cavity.

The designs proposed in the paper are based on ideas originally described in [33], which have been further developed and expanded. To this end, Section II presents a detailed study of a single DM resonant cavity. The operating fundamental and higher-order modes resonating in the cavity along with mode coupling mechanisms are identified and analyzed. Section III describes the whole process of filter design and fabrication. For clarity, a simple fourth-order filter, initially presented in [33], is thoroughly discussed and compared with other solutions in Section III-A. Next, a more challenging design, an eighth-order DM filter composed of four cascaded DM cavities, is presented in Section III-B. The prototype of the filter is fabricated directly in metal using SLM, and measurement results are compared with EM simulation. Our experimentally verified design is compared with other state-of-the-art 3D-printed DM filter solutions, followed by a discussion in Section III-C and concluding remarks in Section IV.

II. RESONANT CAVITY ANALYSIS

A. MODE ANALYSIS

The starting point for this study is a waveguide cavity with a smooth profile, which was adapted for 3D printing [34]. The cavity resonates with the fundamental mode, which is the TE_{110} mode, whose magnetic (H) field distribution is shown in Fig. 1. The mode numbering follows the XYZ coordinate system shown in the figures. Such a single-mode resonant cavity has a constant height and smooth, rounded side walls. To obtain DM operation, the cavity was modified by applying the shape deformation technique. The top and bottom walls of the cavity were stretched vertically

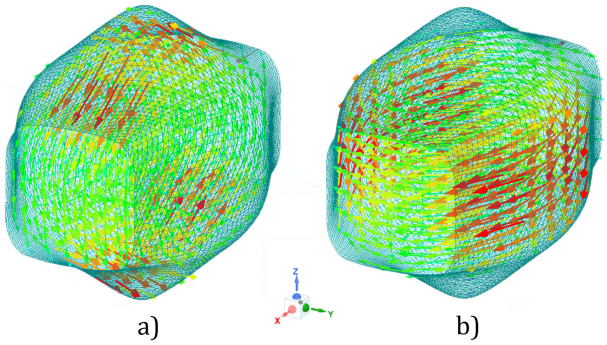

FIGURE 2. Operating fundamental modes (H field) in the deformed (vertically stretched) rectangular waveguide cavity: a) Mode 1: TE101, b) Mode 2: TE110.

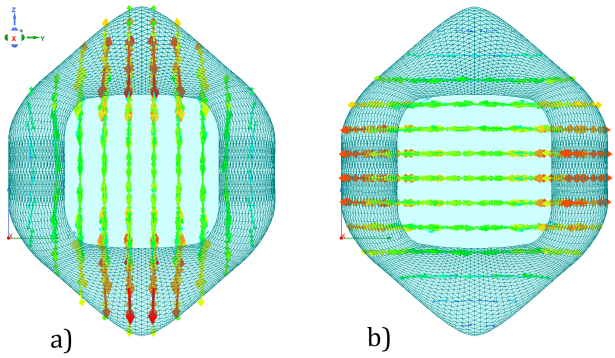

FIGURE 3. Operating fundamental modes (H field) in the deformed (vertically stretched) rectangular waveguide cavity: a) Mode 1: TE101, b) Mode 2: TE110.

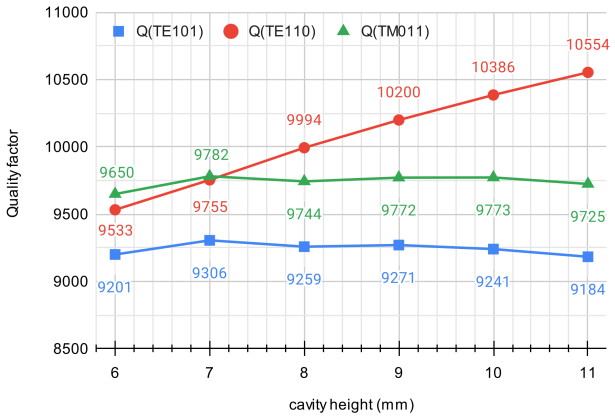

FIGURE 4. Chart showing the influence of cavity height (vertical deformation) on the quality factor of the two operating TE modes and higher-order TM mode. Analysis performed assuming the conductivity of ideal aluminum, $\sigma = 3.8 \cdot 10^7$ S/m.

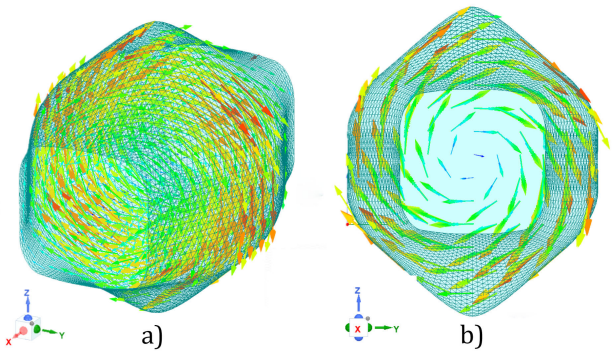

FIGURE 5. TM011 mode (H field) in the deformed rectangular waveguide cavity: a) 3D view, b) side view (YZ plane).

(symmetrically along the Z-axis), allowing the second quasi-TE_{101} mode to resonate in the orthogonal direction, which is illustrated in Fig. 2. A detailed mode analysis was carried out for proper characterization of the resonating modes and constraints imposed by higher-order spurious modes. Eigenmode simulations in Ansys HFSS were performed to determine the resonance frequencies, estimate the unloaded quality factors Q_u, and examine the EM field in the cavity. The results are summarized and compared with a reference spherical cavity in Table 1. The reported Q_u values were calculated for ideal aluminum (electrical conductivity equal to $\sigma = 3.8 \cdot 10^7$ S/m.). The two orthogonal quasi-$TE_{110/101}$ modes resonate at around 12 GHz, yielding a high Q-factor. A cross-sectional view (YZ plane) of the H field distribution of the two fundamental quasi-TE modes operating in the cavity is shown in Fig. 3a and Fig. 3b. The first higher-order mode is the quasi-TM_{011} mode, resonating at about 13.2 GHz, whose H field distribution is provided in Fig. 5. The next higher-order modes are of the TE_{2nm} family, and resonate at around 16.5 GHz.

The influence of vertical stretching on the Q_u of the two operating quasi-TE modes and the quasi-TM mode is shown in Fig. 4. As expected, stretching increases the volume of the DM cavity along one direction, resulting in a slight increase in Q_u for one of the operating modes. Similarly, change of the orthogonal cavity dimension (horizontal) would lead to a similar increase in Q_u for the orthogonal mode. Nonetheless, the Q-factors of all three examined modes remain similar and falling in the range of 9000–10500, assuming ideal aluminum conductivity. These values can be considered a good result as they remain satisfactory albeit the Q_u is degraded by 12–15% with respect to the spherical cavity solution, reported in Table 1.

B. SUPPRESSION OF THE TM MODE

As indicated above, the next higher-order mode excited in such a deformed cavity is the TM_{011} mode. The H field distribution of this mode is illustrated in Fig. 5. This mode can affect the spurious-free operation of the dual-mode cavity. Our numerical tests show that, depending on the cavity shape, the TM_{011} mode can resonate close to both useful TE modes, or even become a fundamental one. In filter applications, maintaining the ideal symmetry prevents the TM_{011} mode from coupling to the TE modes and adding an extra reflection zero in the filter response. However, if the symmetry is broken, it may lead to energy loss visible as a "notch" in

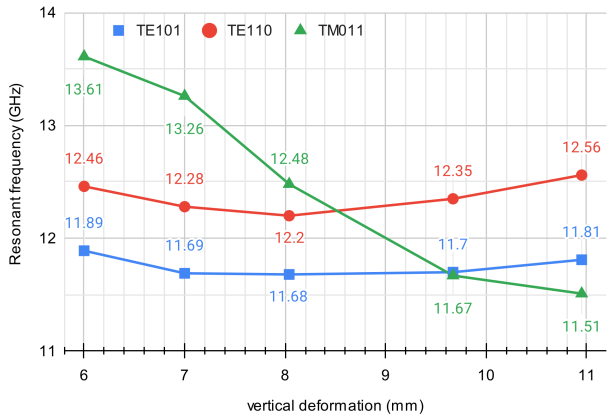

FIGURE 6. Mode chart illustrating the influence of cavity height (vertical deformation) on the two operating TE modes and higher-order TM mode.

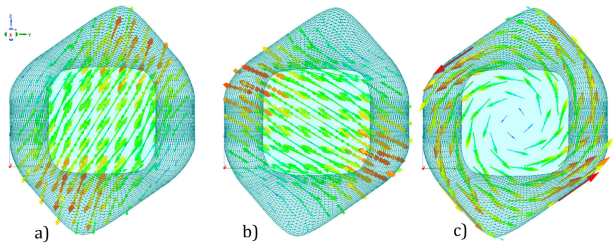

FIGURE 7. Operating modes (H field) in the modified DM cavity: a) Mode 1, b) Mode 2, c) TM mode.

TABLE 1. Mode and Q_u analysis of DM cavity resonators.

cavity type	DM cavity in Fig. 3	Modified DM cavity in Fig. 7	Spherical cavity
fundamental modes, f_r (GHz)	11.83 (TE_{101}), 12.14 (TE_{110})	11.69 (TE_{101}), 12.28 (TE_{110})	11.69 (TM_{101})
first spurious mode, f_r (GHz)	13.23 (TM_{011})	13.26 (TM_{011})	16.48 (TM_{2m1})
fundamental modes, Q_u*	9210 (TE_{101}), 9525 (TE_{110})	9180 (TE_{101}), 9520 (TE_{110})	10885 (TM_{101})

* Q_u given for ideal Aluminum ($\sigma = 3.8 \cdot 10^7$ S/m.).

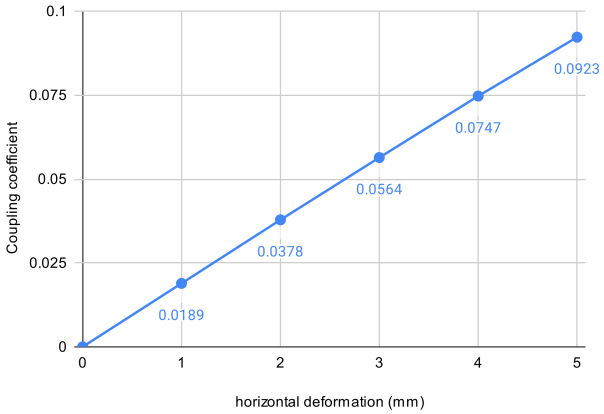

FIGURE 8. Chart demonstrating the variation of the coupling coefficient between the two TE modes operating in the DM cavity vs. horizontal deformation.

or near the passband. Nonetheless, if the resonance occurs outside of the operational band, it is strongly suppressed and would be practically irrelevant to the filter response. Therefore, during the design stage, efforts should be made to keep the TM mode away from the operating frequency range. The resonance frequency f_{TM} is directly associated with the height of the cavity and can be controlled by vertical stretching: the greater the height, the lower the frequency of the spurious mode f_{TM}. This relationship, illustrated by a mode chart in Fig. 6, must be considered to keep the TM mode away from the operating frequency of the fundamental modes. For this reason, we set a limit on the cavity height and followed it during the design process.

C. COUPLING ANALYSIS

Once the modes operating in a single DM cavity are properly arranged, the proposed resonant structure can be used to create a simple two-pole bandpass filter (BPF). To this end, the cavity from Fig. 2 needs to be connected to input and output waveguide sections. Please note that a simple input/output arrangement will not lead to the creation of a two-pole filter, because the cavity is symmetric. The excitation from the input/output (I/O) waveguide operating with the fundamental TE mode will couple only to the horizontal TE_{110} mode, and the second mode, TE_{101}, will not be excited. There are several possible solutions to establish coupling to the other TE mode and achieve effective DM operation in the cavity, resulting in a simple two-pole filter. For instance, coupling screws could be introduced in the cavity to break the symmetry, but such an action would reduce the Q-factor of the cavity and increase the complexity of the design. One could also introduce direct coupling from the source or load to both modes, as was done in [29]. However, such a solution does not introduce internal coupling between the two orthogonal modes, which will be necessary for creating the higher-order BPF configurations that we intend to design. Instead, we propose the two modes to be excited by introducing a horizontal deformation of the cavity (in the Y-axis direction) along with the previously specified vertical stretching operation. Specifically, the two vertices of the structure are moved away from the central axis. This way, the symmetry along the Y-axis is broken, leading to energy exchange between the two modes. The modified DM cavity with the proposed horizontal displacement is shown in Fig. 7. By varying the value of the horizontal deformation, we can control the coupling between the two modes operating in the DM cavity, as shown in Fig. 8. The achievable coupling values allow for the design of a wide range of narrow- and wideband filter responses. In our simulation tests, we have successfully designed filters with fractional bandwidths between 0.65% and 8.7%.

We also performed a mode analysis of the modified resonant structure and compared the results with the symmetrical one in Table 1. We found that this modification does not affect the resonances and Q-factors significantly. The deformation

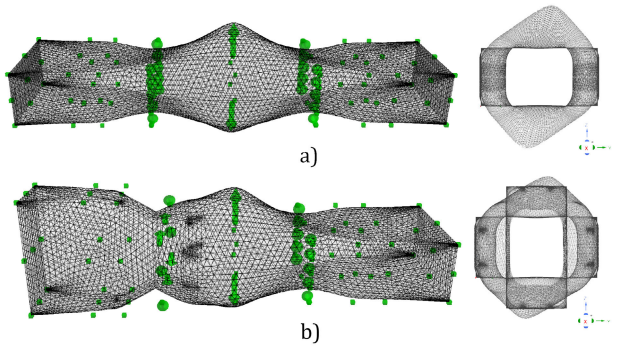

FIGURE 9. Geometry of the resonant cavity with input/output ports: a) modified DM cavity with introduced horizontal offset, b) modified DM cavity with 90-degree rotated output.

slightly rotates the polarization of the two orthogonal modes, as seen when comparing the field distribution in Fig. 7 and Fig. 3. In theory, the mode polarization shift could enable direct coupling from the source or load to the second (orthogonal) TE mode. However, a series of EM simulations were conducted and revealed that such additional coupling is negligible and we can ignore it in the design process. This direct coupling would occur if we rotate the I/O ports relative to the cavity, resulting in the appearance of an additional transmission zero (TZ) close to the passband. This coupling mechanism is well documented and has been successfully applied in [29], but is not used in this work.

The modified version of the DM cavity (with the broken symmetry along the Y-axis) was connected with standard WR-75 waveguide sections, as shown in Fig. 9a. This cavity arrangement aligns the input and output waveguide ports, matching the coupling-routing diagram (CRD) shown in Fig. 10a. In this configuration, both the source and the load are coupled to only one of the two TE modes supported by the cavity, and this mode couples to its orthogonal counterpart via perturbed symmetry. The frequency response of such a structure is not that of a BPF, as it consists of two reflection zeros separated by a TZ. In order to obtain a two-pole BPF response, an inline topology is required. Such a configuration, displayed in Fig. 10b, can be created when the output port is rotated 90° with respect to the input port, as shown in Fig. 9b. This way, the incident EM wave from the input waveguide section excites the first TE mode, and the output section is coupled to the second mode. In all the designs considered in this work, the I/O coupling is controlled by means of inductive irises formed by compressing the side walls of the waveguide sections (as indicated by green arrows in Fig. 9). The modified DM cavity design from Fig. 9b can function as a high-Q, second-order BPF with a smooth profile and a 90° twisted output. Alternatively, the DM cavity can serve as a building block for higher-order filter configurations.

III. FILTER DESIGN

The study of the resonant modes and coupling schemes that are implementable in the proposed cavity presented

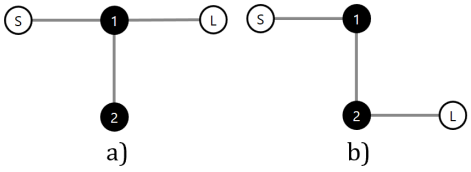

FIGURE 10. Coupling-routing diagram of the modified single-cavity DM filter: a) with the same orientation of input and output waveguide, as shown in Fig. 9a, b) with a 90° rotation of the output, as shown in Fig. 9b.

in the previous section is essential for developing more advanced BPF designs with quasi-elliptic response. In this paper, we examine two such designs in detail. The first one is a fourth-order BPF with a 90° rotated output. This design was presented as a preliminary example in [33]. It offers an advanced filtering function (four-pole response with one TZ) in a compact volume, integrated 90° polarization rotation and high Q-factor, and can be fabricated as a single piece using direct metal AM. The second one is an eighth-order BPF with four TZs, which consists of four cascaded DM cavities interconnected with quasi-square or quasi-elliptical irises. This is a new design aiming for high-power and low-loss applications, and has key features such as compact size, high Q, and high power handling due to its smooth profile. Again, the design is verified experimentally by 3D printing as a single component. All filter prototypes presented in this paper are interfaced with a WR-75 rectangular waveguide and manufactured from aluminum alloy (AlSi10Mg) using the SLM process.

A. FOURTH-ORDER FILTER DESIGN

The first design is a fourth-order BPF consisting of two cascaded DM cavities. The model is built by expanding the single-cavity configuration from Fig. 9b to include a second DM cavity and connecting them via a quasi-square iris. The developed 3D model of the filter and its corresponding coupling-routing diagram are presented in Fig. 11. Each DM cavity supports the resonance of two TE modes, and the quasi-square iris allows coupling to the corresponding modes in the other cavity. Depending on their orientation, the I/O waveguide connections can be coupled to either one of the two modes. The presented asymmetric-box coupling scheme, shown in Fig. 11b, is obtained when the output port is rotated by 90° with respect to the input. This coupling scheme results in a four-pole response with one TZ and offers a 90° rotation of I/O ports at the expense of the additional TZ below passband that would occur if the output port was not rotated.

The design specifications of the filter are: passband 11.25–11.75 GHz (center frequency f_c = 11.5 GHz, bandwidth BW = 500 MHz) and in-band return loss RL > 20 dB. The TZ is positioned close to the passband, at 12 GHz. The passband frequency was chosen to fit within the operating band for the WR-75 waveguide standard, which covers the frequency range of 10–15 GHz. The initial design was optimized following the procedure described in [19] and [34].

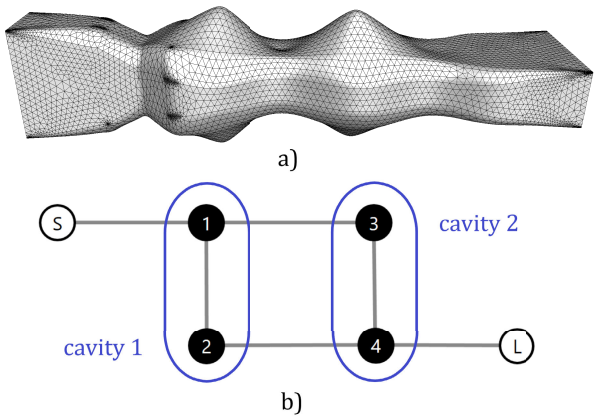

FIGURE 11. Geometry of the fourth-order DM cavity filter: a) 3D model, b) coupling-routing diagram with indicated physical cavities.

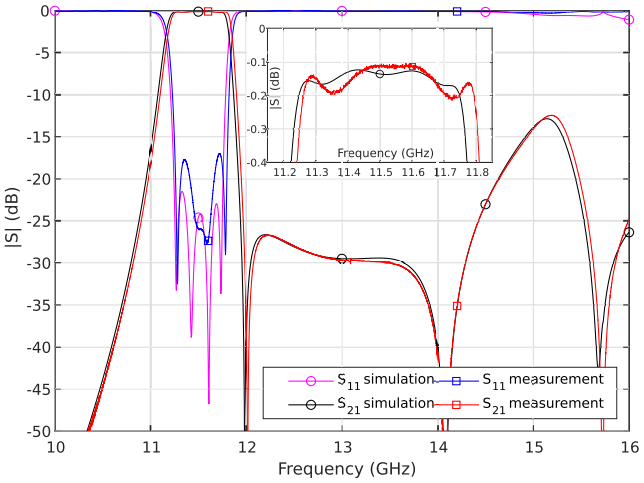

FIGURE 12. Measurement result compared with EM simulation of the fourth-order filter with a 90° output rotation. Inset: close-up view of the in-band insertion loss.

Due to the smoothly contoured nature of the filter, direct analytical synthesis is not feasible. Therefore, the initial synthesis adopts a two-step approach. The first step involves the design of dual-mode deformed cavities to resonate at the specified filter passband. Subsequently, the cavities are coupled, and a comprehensive full-wave optimization was performed. The process involved twelve optimization variables, including two geometric parameters describing the lengths of cavity sections, as well as deformation parameters, i.e., four variables standing for the vertical stretching and horizontal deformation of the cavities, and six variables controlling the shape of the irises. The zero-pole method was used for optimization, as it is a highly effective strategy for microwave filter design [35], [36], [37]. The parameters of the shape deformation based on RBFs were kept fixed: the interpolating function was a polyharmonic spline with power $k = 3$. This type of basis function ensures a very smooth profile of the deformed surface is attained. Additionally, the design optimization imposed constraints on the maximum cavity height to keep the TM modes away from the passband, as discussed in Section II-B.

The EM simulation result of the optimized filter design is presented in Fig. 12. The filter response close to the passband perfectly matches the specification. It should be noted that there is another TZ visible at ca. 14 GHz, and a suppressed resonance occurring at ca. 15 GHz. Eigenmode analysis confirmed that these are associated with the resonance of higher order TE modes. In this case, the additional TZ is beneficial to the design and contributes to good upper stopband rejection up to around 14.5 GHz.

To validate the design, a prototype of the fourth-order filter was manufactured using the SLM process. The filter was 3D-printed as a single piece with no internal supports. The part was oriented vertically in the printing platform, i.e., the printing direction followed the filter's length, from one I/O port to the other. The external dimensions of the printed structure are 90.5 × 38 × 38 mm. The fabricated component was measured using the measurement setup with a vector network analyzer (VNA) and WR-75 waveguide-to-coax adapters, as shown in Fig. 13. The comparison of the measurement and EM simulation results provided in Fig. 12 shows excellent agreement with the simulated model. The measured response is shifted approximately 40 MHz above the specified frequency band, but the in-band and out-of-band behavior is accurately reproduced. The return loss level in the passband is greater than 17 dB, which is a very good result since no tuning was applied to achieve this response. The insertion loss (IL) of the 3D-printed filter is shown in the inset in Fig. 12. It equals 0.11 dB at f_c and varies between 0.1 and 0.2 dB across the passband. This corresponds to the estimated Q of the filter of around 3500. Based on the IL value, we estimated the effective metal conductivity to be equal to $\sigma_{\text{eff}} = 9 \cdot 10^6$ S/m, which is a very good result for a 3D-printed aluminum alloy, considering the surface roughness usually obtained in this fabrication process without additional internal surface postprocessing.

A comparison of the developed fourth-order BPF with other state-of-the-art 3D-printed DM filters is presented in Table 2. Several 3D-printed filters of order $N \leq 4$ with various relative bandwidths fabricated using different AM techniques are included in this overview. Among the compared solutions, the presented filter design exhibits the lowest insertion loss and a very high Q value. This is particularly noteworthy for a component printed directly in metal with no post-processing or tuning.

B. EIGHTH-ORDER FILTER DESIGN

On successful completion of the fourth-order filter prototype, the development of a more challenging design, i.e. an eighth-order BPF with four TZs, was considered in the next step. The structure consists of four DM cavities cascaded one-by-one and coupled together by integrated quasi-rectangular irises, as shown in Fig. 14a. Once again, the filter is developed for 3D printing as a single block with a smooth surface

TABLE 2. Comparison with state-of-the-art 3D-printed dual-mode filters of order $N \leq 4$.

Ref.	Filter order	f_c (GHz)	FBW (%)	IL at f_c (dB)	Q	3D printing technology, material
[38]	4	10.0	3.0	0.25	2500*	SLA, copper-plated
[29]	2	10.0	2.5	0.47	500*	SLA, copper-plated
[27]	4	5.987	3.37	0.6	840	LCM, alumina
[15]	4	11.565	∼0.47	1.0	5800	SLM, Invar, silver-plated
[15]	4	11.483	0.47	1.5	2900	SLM, Invar, silver-plated after tuning
[11]	4	10.8	0.67	1.0	2500	SLM, aluminum
T.W.	4	11.5	4.35	0.11	3500	SLM, aluminum

Ref.: reference, f_c: center frequency, FBW: fractional bandwidth, IL: insertion loss, SLA: stereolithography apparatus, LCM: lithography-based ceramic manufacturing, SLM: selective laser melting, T.W.: this work.
* Q estimated based on available filter specifications and measured IL.

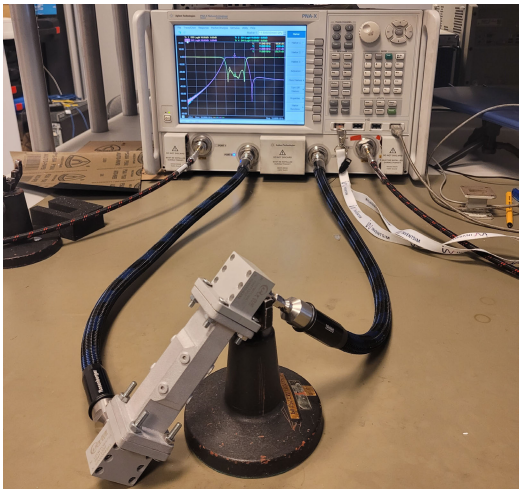

FIGURE 13. Measurement setup using WR-75 waveguide-to-coax adapters.

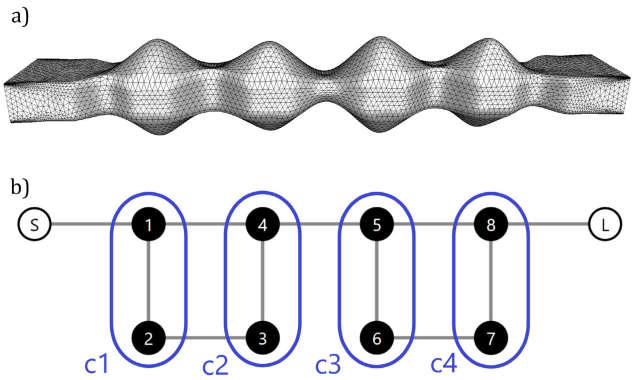

FIGURE 14. Geometry of the eighth-order DM cavity filter: a) EM model created using shape deformation, b) coupling-routing diagram.

profile, so there are no sharp corners or edges found anywhere in this design. The specifications for the new filter match

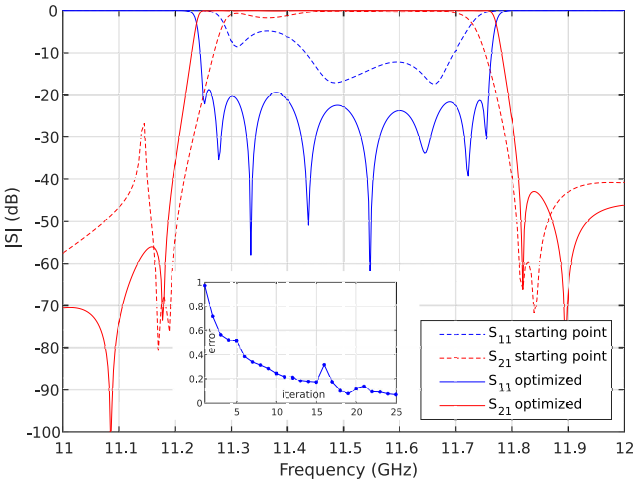

FIGURE 15. Optimization of the eighth-order BPF design: starting point (dashed line), optimized response (solid line). Inset: optimization error in each iteration.

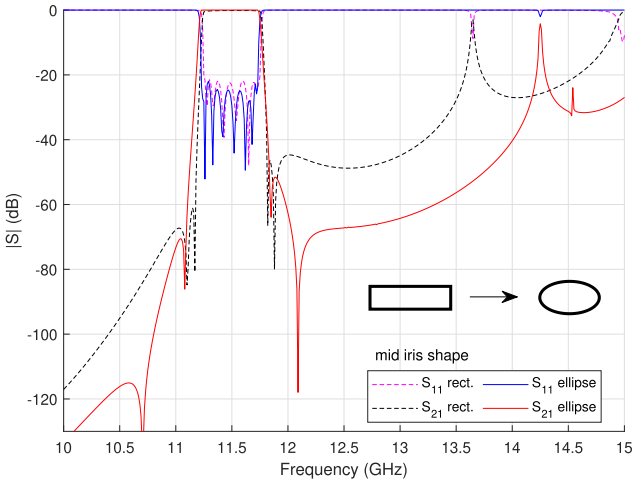

FIGURE 16. Comparison of EM simulation results of the eighth-order filter design with different mid iris shape: rectangular (dashed line) and quasi-elliptical (solid line).

those of the fourth-order design: a center frequency $f_c = 11.5$ GHz, fractional bandwidth (FBW) = 4.35%, and return loss level RL > 20 dB. The arrangement of cavities and irises is represented by a coupling-routing diagram in Fig. 14b, where the physical cavities are indicated by blue oval areas. To implement the chosen filter topology, the irises between cavities No. 1 and 2 and between cavities No. 3 and 4, need to support two couplings of the orthogonal mode pairs. Therefore, in their case, a quasi-square iris shape is used, as was done previously in the fourth-order filter design. In contrast, the middle iris, connecting cavities No. 2 and 3, should allow the coupling of only one pair of TE modes. For this reason, a narrow quasi-rectangular slit was implemented in the initial filter design.

The initial model was optimized using the same approach based on the zero-pole method [19], [37]. In this optimization procedure, the goal function compares the locations of zeros

and poles extracted from the filter's transfer and reflection functions with reference values of the prototype filter. There are 22 parameters used in the process: four variables describing the length of each cavity, ten variables modeling the shape of the irises (two per iris, representing its height and width), and eight parameters controlling the deformation of the cavities. The comparison of the S-parameter response of the initial and optimized design, as well as the obtained error value, can be observed in Fig. 15. The optimized result was reached in 25 iterations, and the computations performed on an Intel Core i9-10900X workstation with 64 GB RAM were completed in less than three hours.

It can be observed that the simulated response of the optimized design, shown in Fig. 16, provides a very poor upper stopband region (plotted with a dashed line). The first spurious resonance, which can be seen at the frequency of ca. 13.6 GHz, is associated with the geometry of the mid iris, and can be controlled by its shape and width. Therefore, the first design was modified so that the out-of-band rejection level could be improved. An improvement was obtained by optimizing the shape of the mid iris into a rounded, elliptical shape, which is shown in Fig. 16 (solid line). The spurious resonance was shifted up to ca. 14.25 GHz, and the rejection level was improved to around 60 dB under 13.25 GHz and around 40 dB up to 14 GHz. In addition, the center frequency in the revised design was shifted down by 20 MHz to $f_c = 11.48$ GHz to anticipate the manufacturing impact on the dimensions of the filter. In this design, the positions of the TZs can also be modified: they can be placed closer to or farther from the passband with little effect on the selected bandwidth. The solution chosen in this study was to place one pair of TZs close to the passband—at 11.1 and 11.85 GHz—and the other pair farther away—at 10.75 GHz and 12.1 GHz—to improve the upper stopband rejection level. Although the TZs are positioned almost symmetrically on either side of the bandwidth, the attenuation of the lower stopband is noticeably higher. This is due to the proximity of the waveguide cut-off frequency, which affects the rejection of the filter below the passband. The designed structure was also analyzed for multipactor effects in Ansys HFSS. The analysis reported no occurrence of multipaction up to a power threshold of 10 kW, which confirmed the validity of using such a solution for high-power applications.

The eighth-order filter design was prepared for fabrication and 3D-printed by Northern Waves AB. The fabricated component is presented in Fig. 17a. The filter was manufactured in one piece using SLM, with powder layer thickness of 30 μm. The structure was printed along its greatest dimension, from one flange to the other. The external dimensions of the printed component are 145.5 × 38 × 38 mm. Physical polishing by sandblasting was applied in post-processing. According to the manufacturer, the process should reduce the surface roughness (Ra) from 8–10 μm as built, down to 4–6 μm. The prototype was measured using the same setup from Fig. 13 and the results were compared with EM simulation. The wideband response of the filter

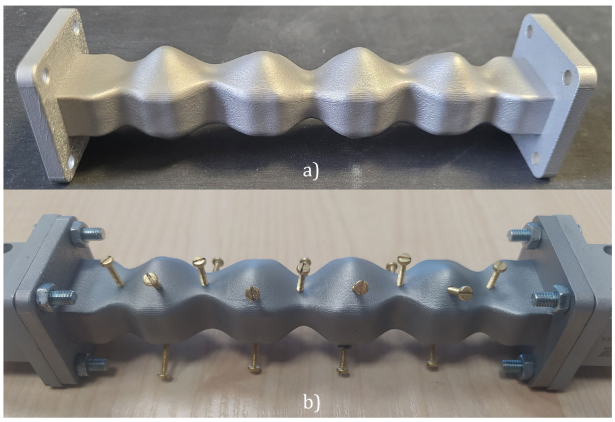

FIGURE 17. Photographs of the eighth-order DM cavity filter: a) 3D-printed filter prototype, b) measured prototype with tuning screws.

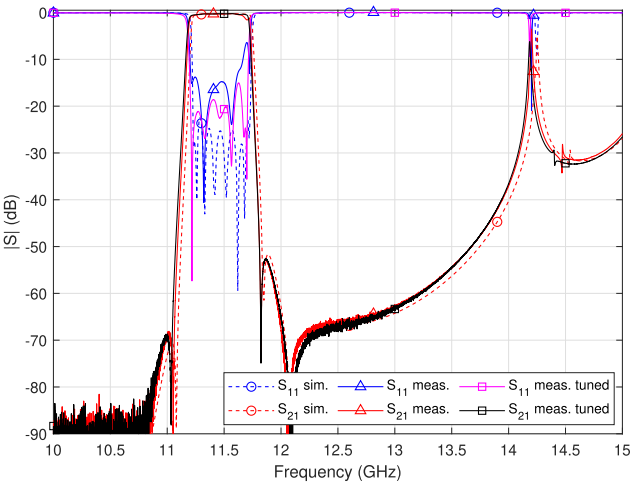

FIGURE 18. Comparison of measurement results (solid line) and EM simulation (dashed line) of the fabricated eighth-order filter with four TZs—wideband response.

is shown in Fig. 18, whereas a close-up of the passband is presented in Fig. 19. There is good agreement with the simulation, although the measured response is shifted ca. 20 MHz below the specified band, and the prototype filter is not fully matched: the return loss is generally better than 15 dB over the passband, apart from the mismatch at the higher edge of the band. The locations of the TZs and the out-of-band response precisely represent the anticipated response. The TZ at the lowest frequency is not visible due to the limited dynamic range of the VNA. Because of the initially unsatisfactory return loss level, tuning screws were incorporated into the cavities and irises, as shown in Fig. 17b, and manual tuning was performed to compensate for manufacturing imperfections, thereby improving the overall in-band RL. A total of 16 tuning screws were used: a pair for each cavity and inter-cavity coupling iris, and one per each I/O iris. The tuned filter response is also shown in Fig. 18 and Fig. 19. The passband insertion loss can be observed in Fig. 20, where the measured response before and after

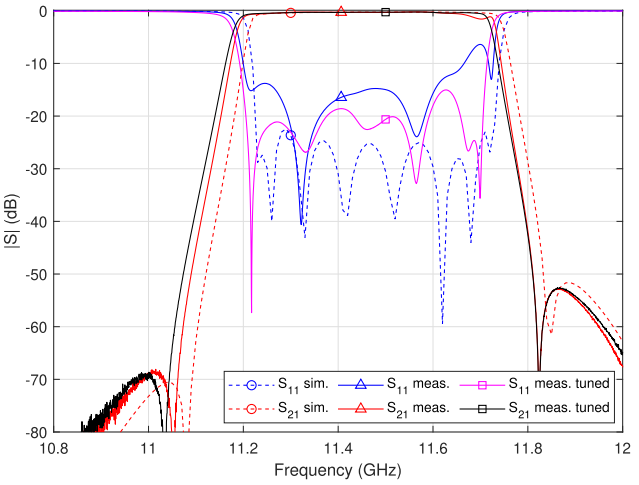

FIGURE 19. Comparison of EM simulation and measurement results of the fabricated eighth-order filter with four TZs—narrowband response.

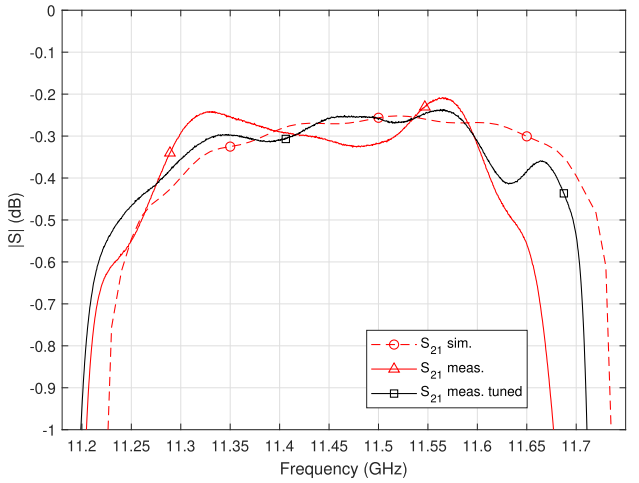

FIGURE 20. Comparison of EM simulation and measurement results of the fabricated eighth-order filter with four TZs—insertion loss.

tuning is compared with the simulation, including conductor losses of the 3D-printed metal surfaces. The IL at f_c is equal to 0.25 dB and spans between 0.25 and 0.55 dB over the passband. This values closely match the simulated effective conductivity of $\sigma_{\text{eff}} = 1 \cdot 10^7$ S/m. The Q of the fabricated filter is estimated as 4500, which is a very satisfactory result for direct metal AM with aluminum alloy. It is also worth noting that the total mass of the component is only 75 g, which is considered a potentially small payload for an eighth-order waveguide filter in the X or Ku-band [38], [39], [40].

A comparison of the proposed eighth-order filter with other 3D-printed filter solutions is presented in Table 3. Our design is listed along with three other BPFs of order $N > 4$ based on DM resonators, with comparable operating frequency and similar or greater FBW. If the Q was not available in the publication, its value was estimated based on the reported IL. Of all the compared solutions, the filter proposed in this work matches the lowest absolute insertion loss, and delivers

TABLE 3. Comparison With State-of-the-art 3D-printed Dual-Mode Filters of Order $N > 4$.

Ref.	Filter order	f_c (GHz)	FBW (%)	IL at f_c (dB)	Q	3D printing technology, material
[41]	6	10.9	7.3	0.7	2000	FDM, copper-coated
[40]	8	8.23	5.47	0.32–0.68	2800*	SLA, copper-plated
[31]	8	8.23	5.59	0.25	5700	SLM, aluminum-copper alloy
T.W.	8	11.46	4.35	0.25	4500	SLM, aluminum

Ref.: reference, f_c: center frequency, FBW: fractional bandwidth, IL: insertion loss, FDM: fused deposition modeling, SLA: stereolithography apparatus, SLM: selective laser melting, T.W.: this work.
* Q estimated based on available filter specifications and measured IL.

a high Q-factor. It has to be noted that a better Q is achieved in [31] by using an aluminum-copper alloy for 3D-printing. Nonetheless, the design presented here represents a viable solution for low-loss, high-power applications.

C. DISCUSSION

The components presented in this article were additively manufactured using the standard SLM process with 30–50 μm resolution, which yielded very satisfactory results for the fourth-order filter model. However, when examining the eighth-order filter prototype, it is clear that the initial measured response (without tuning) did not meet the specifications for in-band return loss. The second design was treated with sandblasting to reduce surface roughness, which in turn decreased the insertion loss and made it possible to obtain a higher Q-factor. However, in order to improve the manufacturing accuracy of the presented prototype and, in consequence, the filter response, more precise 3D-printing methods can be used, such as high-precision micro laser sintering (MLS) with 7 μm layer thickness [42], although this is a considerably slower and more expensive process. Regarding the obtained effective metal conductivity, the estimated value of the 3D-printed aluminum alloy, $\sigma_{\text{eff}} = 1 \cdot 10^7$ S/m, is relatively high compared to the conductivity of ideal aluminum, which is $\sigma_{\text{Alu}} = 3.8 \cdot 10^7$ S/m. However, there are other AM processes reported in the literature involving silver or gold plating of the surfaces, such as [43] and [44], that declare an even more efficient conductivity of $2.5 \cdot 10^7$ S/m. Nonetheless, the fabricated components reported in this paper represent high quality of direct metal 3D printing and validate the design approach based on deformed DM cavities.

IV. CONCLUSION

This article presented a new type of waveguide filter based on deformed dual-mode cavities, designed specifically for 3D printing. The proposed designs were developed using shape deformation and thus benefit from a complex geometry and smooth surface profile, which can only be fabricated by additive manufacturing processes. Fourth-order and eighth-order filters with transmission zeros were

presented and carefully analyzed in this paper. Both filter designs were experimentally verified through prototypes manufactured using the selective laser melting process. The performed measurements validate the design idea and show excellent results compared to the state-of-the-art solutions. The two reported structures exhibit low insertion loss, relatively high Q and a smooth profile, making them potentially useful for low-loss, high-power applications. Although the obtained effective metal conductivity was considered a very good result, further development of additive manufacturing of microwave components along with post-processing techniques, such as polishing [45], or plating [44], should bring even more satisfactory results in the near future.

REFERENCES

[1] P. Booth and E. V. Lluch, "Enhancing the performance of waveguide filters using additive manufacturing," *Proc. IEEE*, vol. 105, no. 4, pp. 613–619, Apr. 2017.

[2] A. I. Dimitriadis, T. Debogovic, M. Favre, M. Billod, L. Barloggio, J.-P. Ansermet, and E. de Rijk, "Polymer-based additive manufacturing of high-performance waveguide and antenna components," *Proc. IEEE*, vol. 105, no. 4, pp. 668–676, Apr. 2017.

[3] T.-H. Chio, G.-L. Huang, and S.-G. Zhou, "Application of direct metal laser sintering to waveguide-based passive microwave components, antennas, and antenna arrays," *Proc. IEEE*, vol. 105, no. 4, pp. 632–644, Apr. 2017.

[4] K. Lomakin, L. Klein, L. Ringel, J. Ringel, M. Sippel, K. Helmreich, and G. Gold, "3D printed E-band hybrid coupler," *IEEE Microw. Wireless Compon. Lett.*, vol. 29, no. 9, pp. 580–582, Sep. 2019.

[5] C. Tomassoni, O. A. Peverini, G. Venanzoni, G. Addamo, F. Paonessa, and G. Virone, "3D printing of microwave and millimeter-wave filters: Additive manufacturing technologies applied in the development of high-performance filters with novel topologies," *IEEE Microw. Mag.*, vol. 21, no. 6, pp. 24–45, Jun. 2020.

[6] P. Vaitukaitis, K. Nai, and J. Hong, "Investigation of metal 3-D printed high-Q multiband waveguide filters using spherical resonators," *IEEE Access*, vol. 12, pp. 1497–1507, 2024.

[7] L. Polo-López, S. Sirci, A. Calleau, S. Capdevila, G. Toso, E. Menargues, and M. García-Vigueras, "Vertically printable evanescent mode filters," *IEEE Microw. Wireless Compon. Lett.*, vol. 32, no. 11, pp. 1299–1302, Nov. 2022.

[8] C. Tomassoni, G. Venanzoni, M. Dionigi, and R. Sorrentino, "Compact quasi-elliptic filters with mushroom-shaped resonators manufactured with 3-D printer," *IEEE Trans. Microw. Theory Techn.*, vol. 66, no. 8, pp. 3579–3588, Aug. 2018.

[9] M. Salek, X. Shang, and M. J. Lancaster, "Compact S-band coaxial cavity resonator filter fabricated by 3-D printing," *IEEE Microw. Wireless Compon. Lett.*, vol. 29, no. 6, pp. 382–384, Jun. 2019.

[10] K. Zhao and D. Psychogiou, "Three dimensional printed vertically-stacked single-/multi-band coaxial filters and RF diplexers," *IEEE Trans. Microw. Theory Techn.*, vol. 71, no. 11, pp. 4957–4968, Nov. 2023.

[11] M. Baranowski, L. Balewski, A. Lamecki, M. Mrozowski, and J. Galdeano, "A circular waveguide dual-mode filter with improved out-of-band performance for satellite communication systems," *IEEE Microw. Wireless Compon. Lett.*, vol. 32, no. 12, pp. 1403–1406, Dec. 2022.

[12] F. Zhang, S. Gao, J. Li, Y. Yu, C. Guo, S. Li, M. Attallah, X. Shang, Y. Wang, M. J. Lancaster, and J. Xu, "3-D printed slotted spherical resonator bandpass filters with spurious suppression," *IEEE Access*, vol. 7, pp. 128026–128034, 2019.

[13] J. Li, C. Guo, L. Mao, J. Xiang, G.-L. Huang, and T. Yuan, "Monolithically 3-D printed hemispherical resonator waveguide filters with improved out-of-band rejections," *IEEE Access*, vol. 6, pp. 57030–57048, 2018.

[14] J. Li, K.-D. Hong, and T. Yuan, "Slotted hemispherical resonators for 3-D printed waveguide filters with extended spurious-free stopbands," *IEEE Access*, vol. 7, pp. 130221–130235, 2019.

[15] L. Qian, Y. Wang, S. Li, A. E. A. Mohamed, M. M. Attallah, T. Skaik, P. Booth, L. Pambaguian, C. M. España, and P. Martín-Iglesias, "A narrowband 3-D printed invar spherical dual-mode filter with high thermal stability for OMUXs," *IEEE Trans. Microw. Theory Techn.*, vol. 70, no. 4, pp. 2165–2173, Apr. 2022.

[16] O. A. Peverini, M. Lumia, G. Addamo, F. Paonessa, G. Virone, R. Tascone, F. Calignano, G. Cattano, and D. Manfredi, "Integration of an H-plane bend, a twist, and a filter in Ku/K-band through additive manufacturing," *IEEE Trans. Microw. Theory Techn.*, vol. 66, no. 5, pp. 2210–2219, May 2018.

[17] C. Bartlett, D. Miek, F. Kamrath, D. Bruhn, and M. Höft, "X-band 3D-printed metal-insert twist-component for bandpass filter applications," in *IEEE MTT-S Int. Microw. Symp. Dig.*, Nov. 2021, pp. 329–331.

[18] J. M. Percaz, J. Hussain, I. Arregui, F. Teberio, D. Benito, P. Martin-Iglesias, I. Arnedo, M. A. G. Laso, and T. Lopetegi, "Synthesis of rectangular waveguide filters with smooth profile oriented to direct metal additive manufacturing," *IEEE Trans. Microw. Theory Techn.*, vol. 71, no. 7, pp. 3081–3101, Jul. 2023.

[19] M. Baranowski, L. Balewski, A. Lamecki, M. Mrozowski, and J. Galdeano, "The design of cavity resonators and microwave filters applying shape deformation techniques," *IEEE Trans. Microw. Theory Techn.*, vol. 71, no. 7, pp. 3065–3074, Jul. 2023.

[20] InventSim. (2023). *EM Invent*. [Online]. Available: http://inventsim.com/

[21] Y. Chen, G. Zhang, J. Hong, Z. Sun, J. Yang, W. Tang, and C. Feng, "3-D printed dual-band filter based on spherical dual-mode cavity," *IEEE Microw. Wireless Compon. Lett.*, vol. 31, no. 9, pp. 1047–1050, Sep. 2021.

[22] P. Vaitukaitis, K. Nai, J. Rao, and J. Hong, "On the development of metal 3D printed bandpass filter with wide stopband based on deformed elliptical cavity resonator with an additional plate," *IEEE Access*, vol. 10, pp. 15427–15435, 2022.

[23] L. Robins, C. Bartlett, A. Arsanjani, A. Widaa, R. Teschl, M. Höft, and W. Bösch, "3D-printed dielectric resonators for quasi-TE_{112} mode singlets, doublets and dual-mode filters," *IEEE Access*, vol. 10, pp. 130326–130338, 2022.

[24] L. Robins, C. Bartlett, A. Arsanjani, R. Teschl, W. Bösch, and M. Höft, "A 3-D-printed dielectric resonator for triple-mode applications," *IEEE Microw. Wireless Technol. Lett.*, vol. 33, no. 11, pp. 1517–1520, Nov. 2023.

[25] D. Miek, P. Boe, and M. Höft, "Additive manufactured dual-mode X-shaped filter realized by high-permittivity ceramics," in *Proc. 15th German Microw. Conf. (GeMiC)*, Mar. 2024, pp. 205–208.

[26] C. Kelleci and A. Atalar, "An analytical approach to the design of multiple mode rectangular cavity waveguide filters," *IEEE Trans. Microw. Theory Techn.*, vol. 65, no. 8, pp. 2857–2865, Aug. 2017.

[27] D. Miek, M. Höft, J. A. Lorente, A. Berger, D. Brouczek, M. Schwentenwein, A. Brandao, P. Martín-Iglesias, and V. T. D. Crestvolant, "Ceramic additive manufactured monolithic X-shaped TM dual-mode filter," *IEEE J. Microw.*, vol. 2, no. 3, pp. 496–506, Jul. 2022.

[28] K. Zhao and D. Psychogiou, "Compact 3D-printed bandpass filters using coaxial and dual-mode ridged-waveguide resonators," in *IEEE MTT-S Int. Microw. Symp. Dig.*, Jun. 2023, pp. 744–747.

[29] E. López-Oliver and C. Tomassoni, "3-D-printed dual-mode filter using an ellipsoidal cavity with asymmetric responses," *IEEE Microw. Wireless Compon. Lett.*, vol. 31, no. 6, pp. 670–673, Jun. 2021.

[30] E. López-Oliver and C. Tomassoni, "Dual-band filters based on dual-mode ellipsoidal cavities," in *IEEE MTT-S Int. Microw. Symp. Dig.*, Jun. 2022, pp. 88–91.

[31] X. Wen, C. Guo, X. Shang, Y. Yu, M. Shu, Q. Yang, S. Li, M. M. Attallah, H. Liu, and A. Zhang, "SLM printed waveguide dual-mode filters with reduced sensitivity to fabrication imperfections," *IEEE Microw. Wireless Compon. Lett.*, vol. 31, no. 11, pp. 1195–1198, Nov. 2021.

[32] P. Savi, D. Trinchero, R. Tascone, and R. Orta, "A new approach to the design of dual-mode rectangular waveguide filters with distributed coupling," *IEEE Trans. Microw. Theory Techn.*, vol. 45, no. 2, pp. 221–228, Feb. 1997.

[33] M. Baranowski, Ł. Balewski, A. Lamecki, and M. Mrozowski, "Rectangular waveguide filters based on deformed dual-mode cavity resonators," in *Proc. 53rd Eur. Microw. Conf. (EuMC)*, Sep. 2023, pp. 400–403.

[34] M. Baranowski, L. Balewski, A. Lamecki, and M. Mrozowski, "Fast design optimization of waveguide filters applying shape deformation techniques," in *Proc. 24th Int. Microw. Radar Conf. (MIKON)*, Sep. 2022, pp. 1–4, doi: 10.23919/MIKON54314.2022.9924969.

[35] P. Kozakowski and M. Mrozowski, "Quadratic programming approach to coupled resonator filter CAD," *IEEE Trans. Microw. Theory Techn.*, vol. 54, no. 11, pp. 3906–3913, Nov. 2006.
[36] A. Lamecki, L. Balewski, and M. Mrozowski, "An efficient framework for fast computer aided design of microwave circuits based on the higher-order 3D finite-element method," *Radioengineering*, vol. 23, no. 4, pp. 970–978, Dec. 2014.
[37] L. Balewski, G. Fotyga, M. Mrozowski, M. Mul, P. Sypek, D. Szypulski, and A. Lamecki, "Step on it bringing fullwave finite-element microwave filter design up to speed," *IEEE Microw. Mag.*, vol. 21, no. 3, pp. 34–49, Mar. 2020.
[38] C. Guo, X. Shang, J. Li, F. Zhang, M. J. Lancaster, and J. Xu, "A lightweight 3-D printed *X*-band bandpass filter based on spherical dual-mode resonators," *IEEE Microw. Wireless Compon. Lett.*, vol. 26, no. 8, pp. 568–570, Aug. 2016.
[39] C. Guo, X. Shang, M. J. Lancaster, and J. Xu, "A 3-D printed lightweight X-band waveguide filter based on spherical resonators," *IEEE Microw. Wireless Compon. Lett.*, vol. 25, no. 7, pp. 442–444, Jul. 2015.
[40] C. Guo, J. Li, J. Xu, and H. Li, "An X-band lightweight 3-D printed slotted circular waveguide dual-mode bandpass filter," in *Proc. IEEE Int. Symp. Antennas Propag. USNC/URSI Nat. Radio Sci. Meeting*, Jul. 2017, pp. 2645–2646.
[41] D. Miek, S. Simmich, F. Kamrath, and M. Höft, "Additive manufacturing of E-plane cut dual-mode X-band waveguide filters with mixed topologies," *IEEE Trans. Microw. Theory Techn.*, vol. 68, no. 6, pp. 2097–2107, Jun. 2020.
[42] T. Skaik, M. Salek, P. Hunyor, H. Wang, P. G. Huggard, P. F. Wilson, M. A. Williams, and Y. Wang, "Evaluation of 3-D printed monolithic G-band waveguide components," *IEEE Trans. Compon., Packag., Manuf. Technol.*, vol. 13, no. 2, pp. 240–248, Feb. 2023.
[43] S. Sirci, E. Menargues, and M. Billod, "Space-qualified additive manufacturing and its application to active antenna harmonic filters," in *IEEE MTT-S Int. Microw. Symp. Dig.*, Nov. 2021, pp. 239–242.
[44] E. De Rijk, M. Favre, M. Billod, A. Dimitriades, and A. Macor, "Procédé de fabrication additive d'un guide d'onde ainsi que dispositifs à guide d'onde fabriqués selon ce procédé," Patent WO 2017 149 423 A1, Sep. 8, 2017.
[45] J. Sorocki, I. Piekarz, M. Baranowski, A. Lamecki, A. Cattenone, S. Marconi, G. Alaimo, N. Delmonte, L. Silvestri, and M. Bozzi, "Low-cost method for internal surface roughness reduction of additively manufactured all-metal waveguide components," *IEEE Trans. Microw. Theory Techn.*, early access, Feb. 12, 2024, doi: 10.1109/TMTT.2024.3361976.

MICHAL BARANOWSKI (Graduate Student Member, IEEE) received the B.Sc. and M.Sc. degrees in electronic and telecommunication engineering from Gdansk University of Technology, Gdansk, Poland, in 2020 and 2021, respectively, where he is currently pursuing the Ph.D. degree with the School of Doctoral. His research interests include computational electromagnetics, microwave filter design, and optimization techniques.

LUKASZ BALEWSKI received the M.S.E.E. and Ph.D. degrees in microwave engineering from Gdansk University of Technology (GUT), Gdansk, Poland, in 2003 and 2009, respectively. He is currently a Lead Programmer of EM Invent. His research interest includes computer aided design of microwave passive components.

ADAM LAMECKI (Senior Member, IEEE) received the M.S.E.E. and Ph.D. degrees in microwave engineering from Gdansk University of Technology (GUT), Gdansk, Poland, in 2002 and 2007, respectively. He is currently the Co-Founder and a CTO of the company EM Invent (Ltd.), which develops the electromagnetic field simulator InventSim. His research interests include filter design and optimization techniques, surrogate models and their application to the computer aided design (CAD) of microwave devices and computational electromagnetics (mainly focused on the finite-element method).

MICHAL MROZOWSKI (Fellow, IEEE) surrogate model construction. He currently serves as a member of the Editorial Board for IEEE Access. He is also a member of the Microwave Theory and Techniques-1 (MTT-1) and MTT-2 Technical Committees, a fellow of the Electromagnetics Academy, and a member of the Polish Academy of Sciences. He was also the past Vice-Dean for research of the Electronics, Telecommunications and Informatics (ETI) Faculty, and the past Chairperson of the Polish Aerospace and Electronic System (AES)/Antennas and Propagation (AP)/MTT Chapter. He served as an Associate Editor for IEEE Microwave and Wireless Components Letters and a member of the Editorial Board for the Proceedings of the IEEE.